Environ Sci Pollut Res (2018) 25:18251–18262
DOI 10.1007/s11356-017-9122-2

Adsorption of terpenic compounds onto organo-palygorskite

Sana Ghrab[1] · **Mabrouk Eloussaief**[1] · **Stéphanie Lambert**[2] · **Samir Bouaziz**[1] · **Mourad Benzina**[1]

Received: 11 January 2017 / Accepted: 26 April 2017 / Published online: 13 May 2017

Abstract Essential oils from aromatic plants are currently mentioned as suitable tools for excellent protection of stored grains from insect pest attacks. The present work aimed to study the processes of the synthesis insecticidal formulation with clay. The active terpenic compounds of essential oil of *Eucalyptus globulus* (Eg) were fixed in the palygorskite by adsorption process. Two sample types of palygorskites were used: raw and organo-palygorskite. The palygorskite clays were characterized by different physicochemical techniques including X-ray diffraction (XRD), Fourier transform infrared (FTIR) analyses, thermogravimetric analysis (TG), differential thermal analysis (DTA), Brunauer-Emmet-Teller (BET), and scanning electron microscope (SEM). Results reveal that the raw clay has a fibrous structure with impurities essential calcite. These structures and physicochemical properties of raw palygorskite and organo-palygorskite give it the potential of material adsorbent. Results show that the adsorption capacity strongly depends on affinity between terpenic compounds and organic cations rather than on interlayer distance of organo-palygorskite. The highest adsorption capacity of terpenic compounds is acquired with palygorskite interlaced by didodecyldimethylammonium bromide (DDDMA). These results validated the potential utility of the Paly-DDDMA as adsorbent fibrous clay for the retention of terpenic compounds in application of environmental preservation.

Keywords Terpenic compounds · Essential oil · Adsorption · Palygorskite · Organo-palygorskite · Environmental application

Responsible editor: Guilherme L. Dotto

✉ Sana Ghrab
ghrab.sana@yahoo.fr

[1] Laboratoire « Eau, Energie et Environnement » (LR3E; code: LR99ES35), Ecole Naionale d'Ingénieurs de Sfax, Université de Sfax, B. P. W, 3038 Sfax, Tunisia

[2] Laboratoire de Génie Chimique, B6a, Université de Liège, 4000 Liège, Belgium

Introduction

Many plants such as Aromatic plants produce terpenic compounds (TC) diffusing into the atmosphere and the soil. This TC are necessary for two reasons: the initial is a cooperation with other species, to seduce pollinating insects or the auxiliaries of the phytophagous insect (Paré and Tumlinson 1996) and antagonistic fungi (Duke 1990); the next admits of an elaboration of dissuasive substances to repel to pest organisms such as insects, pathogenic, microorganisms (Berenbaum 1995), and competitive plants (Duke1990). Otherwise, the function of the protection plant is performed by essential oils. The essential oils are volatile, aromatic oily liquids; natural products with terpenic structure are described by an intense smell. Hence, it is necessary to use the essential oil with her important insecticidal activity in environmental application.

The palygorskite was selected as a good adsorbent for fixed TC. It is clay minerals that together with sepiolite form the group of fibrous clay minerals. The structure of palygorskite was first proposed by Bradley, who described a theoretical formula of $[Si_8\ Mg_5\ O_{20}\ (OH)_2]\ (H_2O)_4 4H_2O$ (Bradley 1940). The palygorskite has a high surface area, moderate cation exchange capacity (Galan1996), and abundant number of silanol groups on palygorskite surface. In other words, palygorskite is a hydrated magnesium silicate mineral with fibrous structure and possesses rectangular channels contained

exchangeable cations, zeolitic water, and water molecules bound to coordinative unsaturated metal ion centers, which situated at the edges of the ribbons (Bradley 1940). Further, raw palygorskite is highly hydrophilic, which has permanent negative charges (Ozcan et al. 2005). Hence, the intercalation of cationic surfactants is needed to reverse its surface charge.

In this study, palygorskite from Gafsa, Tunisia, was selected to adsorb TC from essential oil of *Eucalyptus globulus*. The TC was fixed on various palygorskite adsorbent (raw palygorskite and organo-palygorskite); thanks to the co-adsorption process. To understand the adsorption mechanism, the characterization of raw palygorskite, organo-palygorskite, and kinetic study was determined.

Materials and methods

Chemical materials

Two quaternary ammonium halides leading long alkyl chains have been used for intercalated palygorskite: the hexadecyltrimethylammonium bromide (HDTMA) (96% pure, provided by Fluka Analytica) and didodecyldimethylammonium bromide (DDDMA) (98% pure, provided by Fluka Chemika).

Adsorbate

The essential oil of *E. globulus* was purchased from Aromessence Society located in Tunisia. The essential oil was recovered by hydrodistillation using a modified Clevenger-type apparatus. The essential oil of Eg was kept at 4 °C in a sealed brown vial until its use.

Synthesis of the organo-palygorskite clay

Palygorskite was obtained from Gafsa, Tunisia. The organo-palygorskites were subsequently synthesized according to a combined procedure previously described (Jarraya et al. 2010; Dammak et al. 2014). Raw palygorskite (Paly) was purified by sedimentation and the <2 μm fraction was collected and dried for 48 h at 60 °C. The sample of Paly was ground through a 200 mesh sieve and sealed in a glass tube for use. Ten grams of Paly was dispersed in 1000 mL of NaCl solution (1 M) and stirred at about 1050 rpm for 24 h. Several washing of Na-Paly were performed until a negative test of $AgNO_3$.

Then, 10 g of Na-Paly powder was primary firstly dispersed in 1000 mL of distilled water. The whole was maintained under agitation for 1 h before organic modification. HDTMA and DDDMA are used for the easy exchange with the inorganic compensator exchangeable cations Paly (He et al. 2014). Two CEC (cationic exchange capacity) of HDTMA or DDDMA solutions were then added to Na-Paly dispersions (under stirring) at a flow rate of 3.5 mL/min peristaltic pump. The resulting dispersions were aged at room temperature for 24 h. After intercalation reaction, the solutions were washed several times with distilled water so as to remove excess of organic cations. The obtained clays were finally dried for 24 h at 6 °C and ground in an agate mortar in order to obtain a fine powder.

Characterization

The mineralogical analysis of Paly was carried out by XRD (Philips X'Pert Diffractometer) on the powder of total rock and the oriented aggregates; normal (N) was treated with ethylene glycol (T) and heated at 500 °C for 2 h (H). The XRD spectrum of oriented aggregates. Fourier transform infrared (FTIR) transmittance measurements were carried out between 600 and 4000 cm^{-1} on a Nexus 870 FTIR spectrophotometer according to ATR technical. Specific area was determined by Brunauer-Emmet-Teller (BET) method (micrometrics ASAP 2020 V3.04 H) after degases of 1 g of sample. The gravimetric analysis was realized by analysis of 0.1 g of sample by TGA Q500 V20.13 Build 39. The morphology of Paly was observed by scanning electon microscopy (SEM) (Hitachi S-4500, resolution of 1.5 nm at 15KV).

Adsorption

Essential oil of Eg is rich in TC (Batish et al. 2008). The aim of this part of the work is to interpret the fixation of TC of Eg essential oil onto raw palygorskite (Paly) and organo-palygorskite (Paly-HDTMA, Paly-DDDMA) through adsorption processes.

The kinetic of adsorption was determined by batch reactor in stoppered Pyrex tubes. Firstly, kinetic study was carried out in described tubes containing 10 mL of an Eg solution diluted to 1/20 in acetone, a constant mass of 50 mg of Paly, Paly-HDTMA, and Paly-DDDMA. The adsorbed amount of TC was quantified after 0, 1, 2, 5, 8, 16, and 24 h.

Subsequently, after the realization of the equilibrium adsorption experiment, the dispersions were filtered and the equilibrium concentration of TC (the equilibrated supernatant phase) was determined by gas chromatography (GC-FID). The gas chromatography (Shimadzu type) used was equipped with a flame ionization detector (30 mL of hydrogen, 300 mL of air, 30 mL of nitrogen) and with a column HP-SM (5% phenyl methyl siloxane) (Agilent), length 30 m, diameter 250 μm, film 0.25 μm). The gas carrier was nitrogen with a flow rate of 1 mL min^{-1}. The range of temperature was between 40 and 230 °C at 5 °C min^{-1}, 280 °C at 30 °C min^{-1} and between 230 °C and then it was maintained at 280 °C for 5 min. The injector and detector were maintained at 250 and 280 °C, respectively. The injection was done in split mode with a split ration of 1/10. Adsorption kinetic was determined

using external calibration for each compound of the essential oils. The adsorbed amount was calculated as (Eq. 1):

$$q_t = \frac{n_0 - n_t}{m} \quad (1)$$

where

n_0 is the mmoles of TC in the initial solution of essential oil
n_t is the mmoles of TC in the supernatant
m is the amount of adsorbent (g)

Kinetic studies

Pseudo-first-order model

The pseudo-first-order rate expression of Lagergren is usually described by the following equations (Eqs. 2 and 3) (Srihari and Das 2008):

$$\frac{dq_t}{d_t} = K_1(q_e - q_t) \quad (2)$$

where

q_e is the amount of TC adsorbed at equilibrium time at equilibrium time (mmol g^{-1})
q_t is the amount of TC at time t (mmol g^{-1})
K_1 is the rate constant of pseudo-first-order adsorption (l h^{-1})

Integrating and applying the boundary condition, $t = 0$ and $q_t = 0$ to $t = t$ and $q_e = q_t$ Eq. 1 takes the following form (Eq. 3):

$$\frac{1}{q_t} = \frac{K_1}{q_e t} + \frac{1}{q_e} \quad (3)$$

where the constant K_1 had determined from the slope of linear plots of $1/q_t$ against $1/t$.

Pseudo-second-order model

The adsorption result had analyzed by pseudo-second-order kinetic model by the following Eq. 4. (Wu et al. 2001; Antonioa et al. 2007):

$$\frac{dq_t}{d_t} = K_2(q_e - q_t)^2 \quad (4)$$

where

q_t is the adsorption capacity at time t (mmol g^{-1})
K_2 is the constant of pseudo-second-order adsorption (g $mmol^{-1}$ h^{-1})

Integration and applying the boundary condition, $t = 0$ and $q_t = 0$ to $t = t$ and $q_e = q_t$.

Equation 4 takes the form (Eq. 5):

$$\frac{t}{q_t} = \frac{1}{K_2 q_e^2} + \frac{1}{q_e} t \quad (5)$$

If the second-order kinetic model is applicable, the plot of t/q_t against t of Eq. 5 should give a linear relationship from which the rates q_e and K_2 can be established.

Intraparticulaire diffusion model

The intraparticulaire diffusion approximate recapitulate by Allen et al. (1989) can be practiced. In adsorption mechanism, there is the possibility that the intraparticulaire diffusion is the rate limiting step. The rate constants of the intraparticle diffusion (K_3) are determined using Eq. 6.

$$q_t = K_3 t^{1/2} + C \quad (6)$$

where

q_t is the adsorption capacity at time t (mmol g^{-1})
K_3 is the intraparticulaire diffusion rate constant (mol g^{-1} $h^{1/2}$)
C is the intercept

Results and discussions

Mineralogical analysis

Diffractograms recorded on the powder total rock (Paly) and oriented aggregates (normal (N) were treated with ethylene glygol (T) and heated at 500 °C for 2 h (H)) are presented (Fig. 1) and allow to determine the mineralogical composition of Paly given in Table 1. The raw clay Paly is mainly composed of palygorskite (43%) associated to kaolinite (5%), smectite (1%), calcite (40%), quartz (6%), dolomite (3%), and feldspath (2%) (Table 1).

The XRD patterns of raw palygorskite (Paly) and organo-palygorskite (Paly-HDTMA and Paly-DDDMA) are shown in Fig. 2. In general, no obvious changes on the XRD patterns were mentioned between raw and organo-palygorskites, and the changes of the (110) reflection position were also minor. Subsequently, Paly, Paly-HDTMA, and Paly-DDDMA revealed corresponding reflections at 10.352, 10.350, and 10.425 Å, respectively. Thus, modification with organic surfactants did noticeably difference in the structure of palygorskite during the intercalation process and the surfactants had to move not only through the pores of the Paly but also through channels and they replaced exchangeable

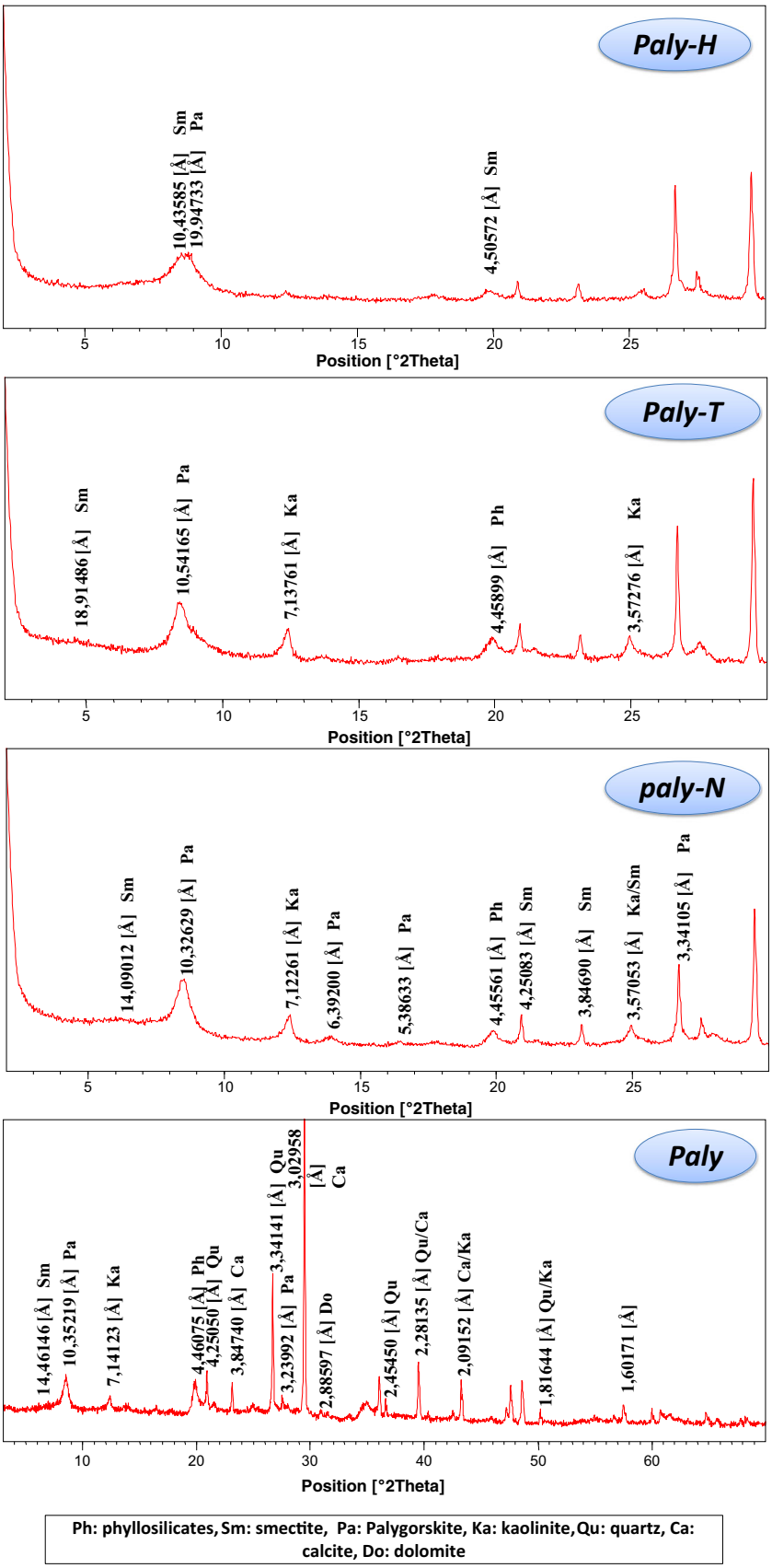

Fig. 1 Diffractograms of total rock and oriented aggregates (N, G, H) of raw palygorskite (Paly)

Table 1 Mineralogical composition of raw palygorskite (Paly)

	Total rock mineralogy (weight %)						
	Clays minerals			Non clay minerals			
	Palygorskite	Kaolinite	Smectite	Calcite	Quartz	Dolomite	Feldspath
Paly	43	5	1	40	6	3	2

cations. The cationic surfactants bind also on the surface of the rod-like crystals can reduce the aggregation of the particle (Yuan et al. 2007).

Physical analysis

The FTIR spectra of Paly, Paly-HDTMA, and Paly-DDDMA are reported in Fig. 3. The band between 3000 and 4000 cm^{-1} of Paly is the results of hydroxyl groups which are coordinated to the octahedral magnesium end the tetrahedral silicon (Han et al. 2015). The band at 3646 cm^{-1} for Paly has been attached to the symmetric modes of molecular water coordinated to the magnesium (or alternative cations of Paly) at the edges of the channels. Bands in the 1200–400 cm^{-1} area are characteristic of silicate; the band at 1000 cm^{-1} for Paly has been associated to the asymmetric stretching modes of Si-O-Si (Balan et al. 2001). The O–H bending band appears at 929 cm^{-1} (Eloussaief et al. 2011). Compared to modified peaks of Paly, there is a supplementary adsorption peak 2938 cm^{-1}, which can be associated to antisymmetric C–H stretching of the terminal CH_3^- groups (Lee and Kim 2002; Tuccimei et al. 2015). These results indicate that HDTMA and DDDMA were been successfully introduce onto Paly.

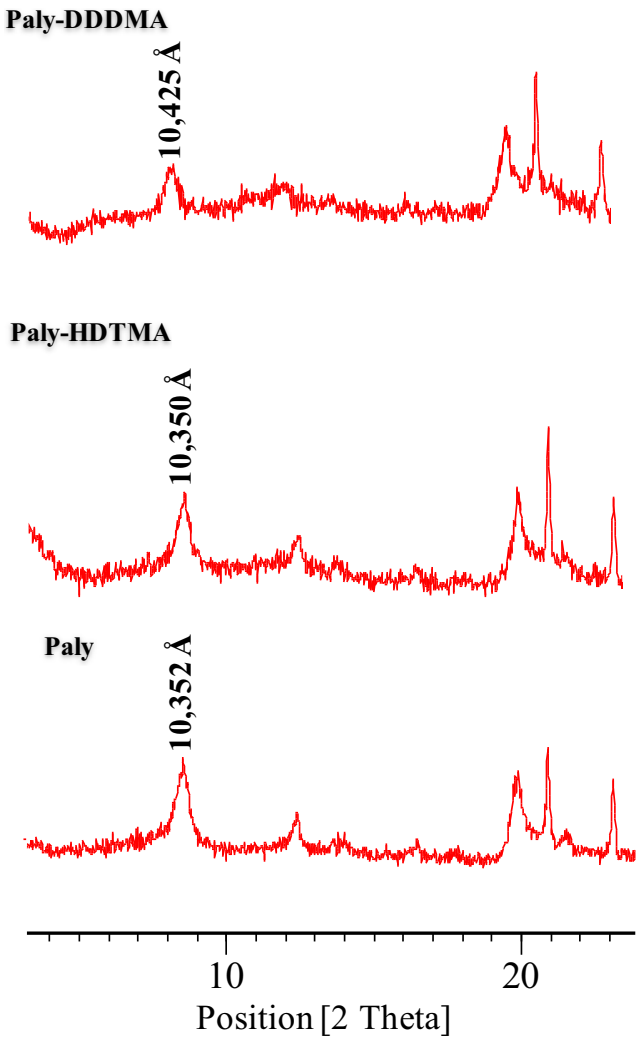

Fig. 2 Diffractograms of raw palygorskite (Paly) and organo-palygorskites (Paly-HDTMA, and Paly-DDDMA)

Textural analysis

The nitrogen adsorption-desorption isotherms of raw palygorskite and organo-palygorskite are shown in Fig. 4, and the BET-specific surface areas are listed in Table 2. The isotherm profiles were classified as type III behavior in the classification of Brunauer, Deming, Deming, and Teller (BDDT) (Brunauer et al. 1940). The curves of raw palygorskite and organo-palygorskite have no obvious hysteresis loops as the curve of smectite clay (Park et al. 2011; Affouri et al. 2015). The saturation of our samples Paly by N_2 is not found. This analysis confirms the structure of paly and is compound by fragile palette developing pore channels.

The BET surface area (S_{BET}) and pore volume (P_V) of samples decrease in order Paly > Paly-HDTMA > Paly-DDDMA. This is expected due to the attachment of HDTMA and DDDMA to the internal frame work of raw Paly causing the constriction of pore channels and the reduction in BET surface area (Juang et al. 2002). The pore size (P_S) of Paly increases after intercalation of HDTMA and DDDMA. Further, the pore size is also involved in the loading of surfactant and modified Paly great surfactant loadings have a larger pore size than that with low surfactant loadings. Similar result was reported for other surfactant-modified adsorbents such as barely straw (Ibrahim et al. 2009; Hamza et al. 2014).

Thermal analysis

Coupled diagrams of differential thermal analysis (DTA) and thermogravimetric analysis (TC) of Paly are shown in Fig. 5.

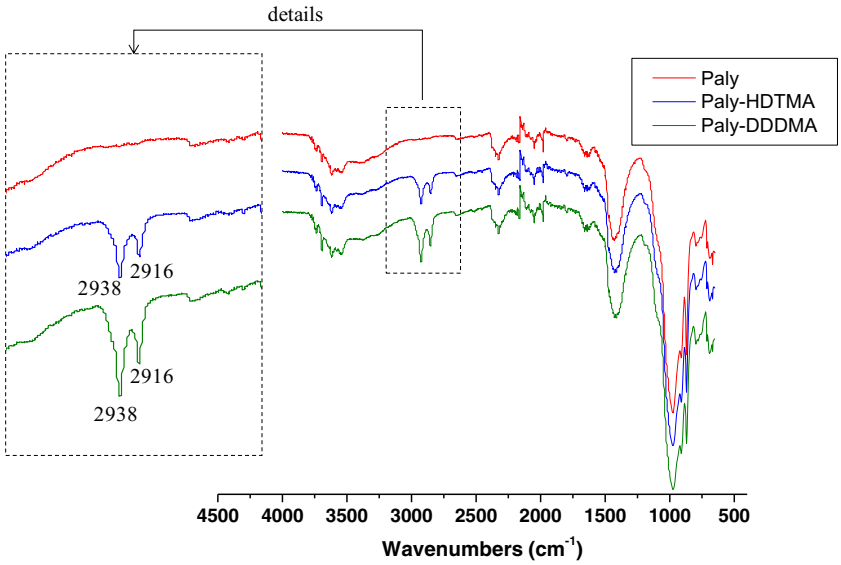

Fig. 3 FTIR spectra of raw palygorskite and organo-palygorskites (Paly, Paly-HDTMA, and Paly-DDDMA)

They show the appearance of a peak at 112 °C, associated by a loss of mass equal to 4.393% accompanied by a loss of mass equal to 4.393% revealing the depart of the moisture and zeolitic water (Callière et al. 1982; Brown 1988). Second peak appeared at 220 °C, accompanied by a loss of mass equal to 7.729% revealing the removal of constitution water resulting from the déshydroxylation of Paly. Another peak is presented at 507 °C, associated to a loss of mass equal to 11.53% reviling the destruction of calcite and dolomite (Xi et al. 2010), major asocial mineral in Paly as mentioned in XRD analysis.

As an additional analysis to the study of organo-palygorskite (Paly-HDTMA and Paly-DDDMA) properties, Fig. 6 shows the TG plots of palygorskite and organo-palygorskite at temperature around 100 °C, a low increase of a loss mass of Paly-HDTMA and Paly-DDDMA, compared with Paly. The water molecules are substituted by HDTMA and DDDMA molecules. Therefore, the surface water content is obtained for the organo-palygorskite, attesting her hydrophobicities (Khalaf et al. 1997; Zhu et al. 2016). A possible justification is that the surface energy of the Paly is weakened by surfactant cations and they explant the hydrophilic clay surface of Paly to an organophilic (Marras et al. 2007). According to this hypothesis, mass loss acquired between 100 and 600 °C should be reported to the decomposition of the surfactant cations (Zhou et al. 2009).

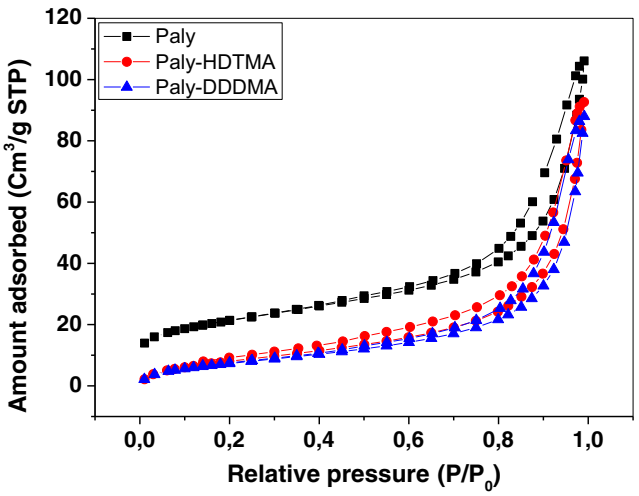

Fig. 4 N_2 adsorption/desorption isotherms of raw palygorskite and organo-palygorskites (Paly, Paly-HDTMA, and Paly-DDDMA)

Morphology analysis

SEM micrographs (Fig. 7) show the surface morphology of palygorskite (Paly) and the organo-palygorskite (Paly-HDTMA and Paly-DDDMA). The rod-like particles were randomly oriented network, densely with variable thickness and length. The characteristic morphology of Paly was similar to those mentioned in some other studies (Yuan et al. 2007; Qiu et al. 2015). The cubic particles of calcite were coated with needles of palygorskite. The associated morphology of palygorskite and calcite is in

Table 2 BET specific area (S_{BET}), pore volume (V_p), and pore diameter (S_p) of raw palygorskite and organo-palygorskite

	S_{BET} (m^2/g)	Vp (cm^3/g)	(P_S) (Å)
Paly	75	0.136	72.344
Paly-HDTMA	32	0.104	130.147
Paly-DDDMA	29	0.098	135.958

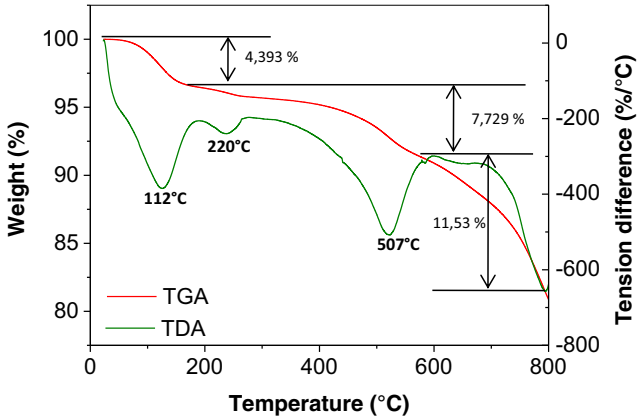

Fig. 5 Diagrams TDA/TGA of raw palygorskite (Paly)

agreement with the result of XRD analysis. After loading with alkylammonium, the SEM images of Paly-HDTMA and Paly-DDDMA were almost unchanged from that of Paly. Again, exhibiting a rod structure with the only exception being the single fibers was coarser.

As shown in Fig. 7, more single fibrous particles were shown on the organo-palygorskite and similar results are proven by (Xi et al. 2010; Wang and Wang 2016). The type of surfactant cations had a strong effect on the morphological changes of palygorskite. The Paly-HDTMA showed more single fibrous particles than Paly-DDDMA. HDTMA cations with one long chain can isolate palygorskite rods from crystal bundles and aggregates. In conclusion, compared with Paly, fibers were frequent and much easier to be showed after modification and they also had more open pore space and were less compacted.

Kinetic studies

The adsorption kinetics informing the rate of the TC (4-methyle-2-pentyle acetate, alpha-pinene, 1,8 cineol, isopinocarveole, beta-humulene, caryophyllene) retention is one of the key features explaining the adsorption ability. The time curves of TC adsorption for the investigated palygorskites are shown in Fig. 8. The adsorption mechanism is rapid at the beginning of the reaction due to the adsorption of TC on the surface sites of palygorskite, and then, it becomes slow due to the diffusion of TC from the surface sites to the fibrous layer of the clay. Therefore, experimental results indicate that the maximum amount of adsorption is reached after 5 h. In order to exploit the adsorption mechanism, the adsorption profiles were fitted with three models: the pseudo-first-order adsorption, the pseudo-second-order adsorption and the intraparticulaire diffusion models.

The results of the kinetic studies of the first order are shown in Fig. 9 and the results of the kinetic studies of the second order are shown in Fig. 10. The value coefficients of all TC adsorbed by Paly, Paly-HDTMA, and Paly-DDDMA were calculated. These constants checked the correlation of kinetic studies with the pseudo-second-order kinetic model (Table 3).

The most correlation of the pseudo-second-order kinetic model is mentioned for Paly-DDDMA. The correlation coefficient for the pseudo-second-order kinetic model was near 0.90, indicating the adsorption of TC by Paly-DDDMA absolutely in agreement with pseudo-second-order kinetic model (Torres-Pérez et al. 2008). Similar results were reported for the other adsorbents by natural clay (Ghrab et al. 2014).

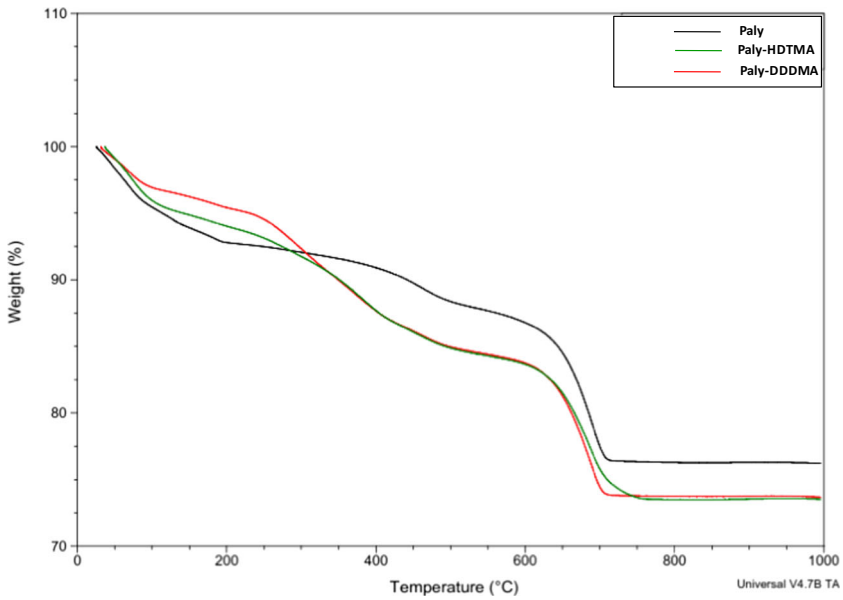

Fig. 6 Diagrams TGA of raw palygorskite and organopalygorskites (Paly, Paly-HDTMA, and Paly-DDDMA)

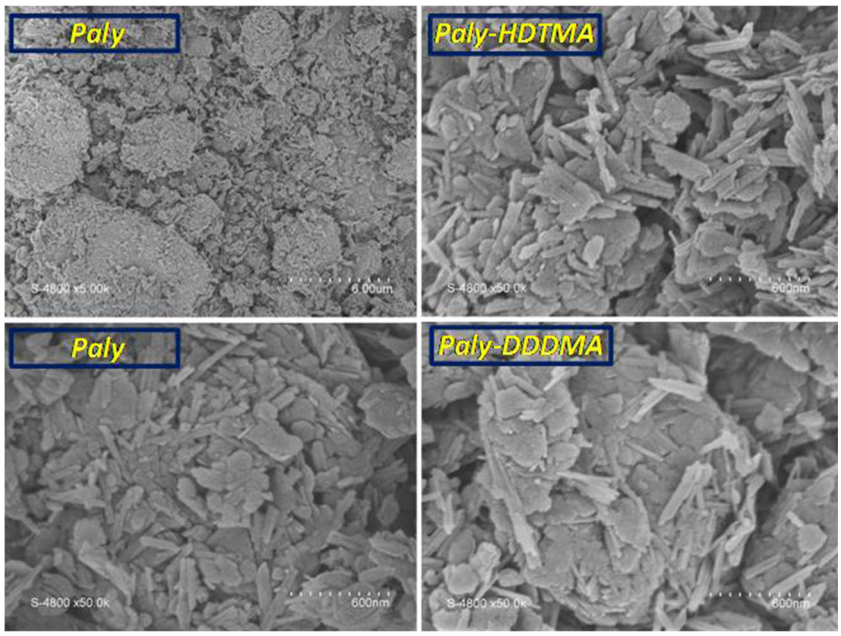

Fig. 7 SEM micrographs of raw an organo-palygorskite (Paly, Paly-HDTMA, and Paly-DDDMA)

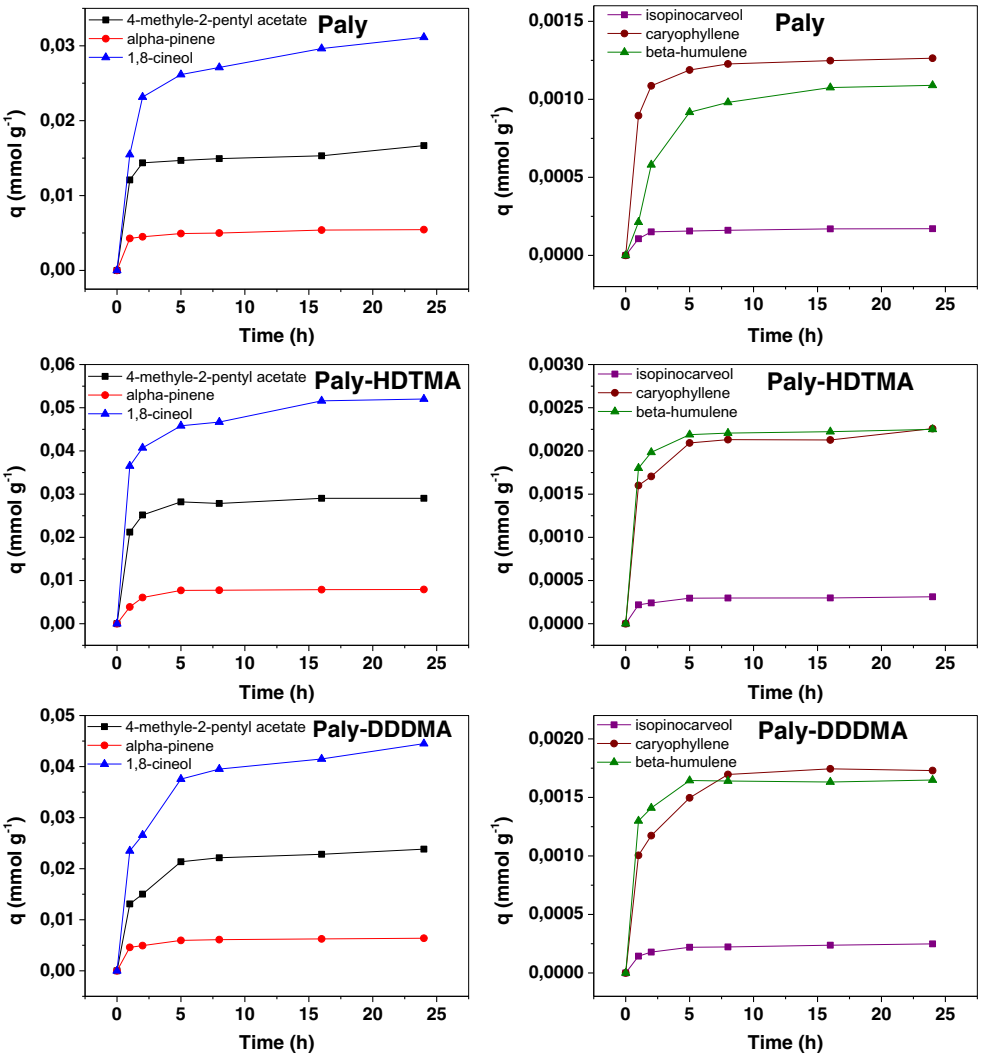

Fig. 8 Effect of contact time on TVOC adsorption onto raw palygorskite and organo-palygorskites (Paly, Paly-HDTMA, and Paly-DDDMA)

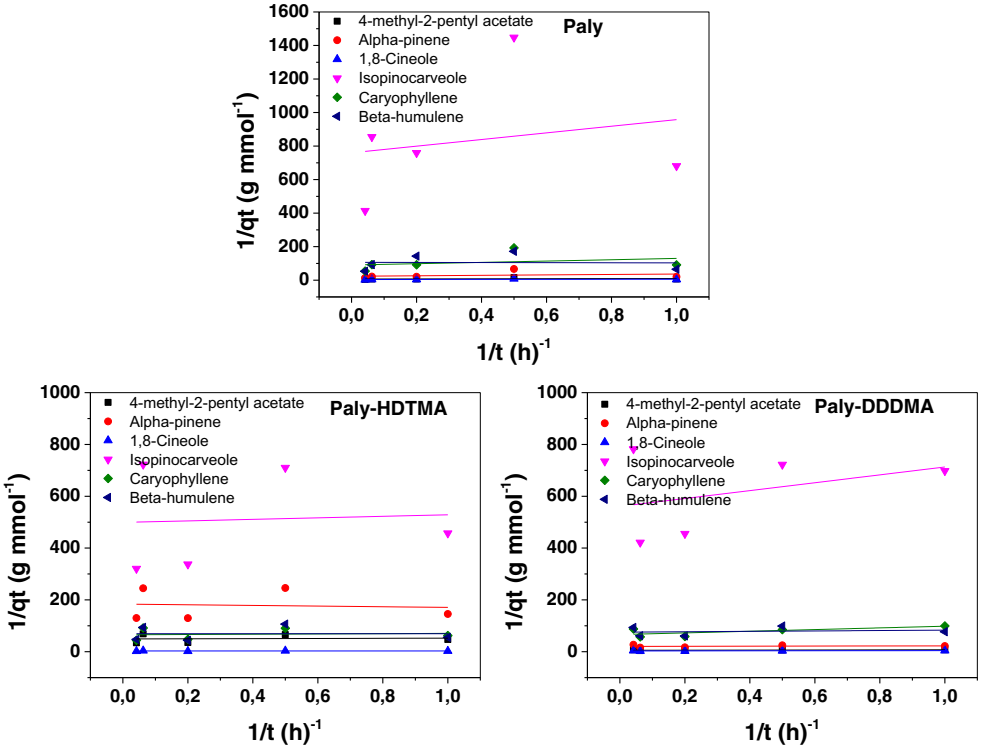

Fig. 9 Kinetics of pseudo-first-order model of raw palygorskite and organo-palygorskite (Paly, Paly-HDTMA, and Paly-DDDMA)

Furthermore, the theoretical q_e values acquired from the second order kinetic are in accordance with the experimental q_e values. Further, the adsorption constant rate expressed by K_2 is improved by the sample Paly-DDDMA for all compounds TC (Hassan et al. 2008). The maximum of adsorption capacities of TC is recorded for Paly-DDDMA. Despite the interfoliaire space is not increasing and the lowest S_{BET} is mentioned for Paly-DDDMA. For two reasons, firstly, the higher DDDMA molecules substitute the zeolitic water and some exchangeable cations in the channels of palygorskite. It is filled the empty and created a new adsorption sites.

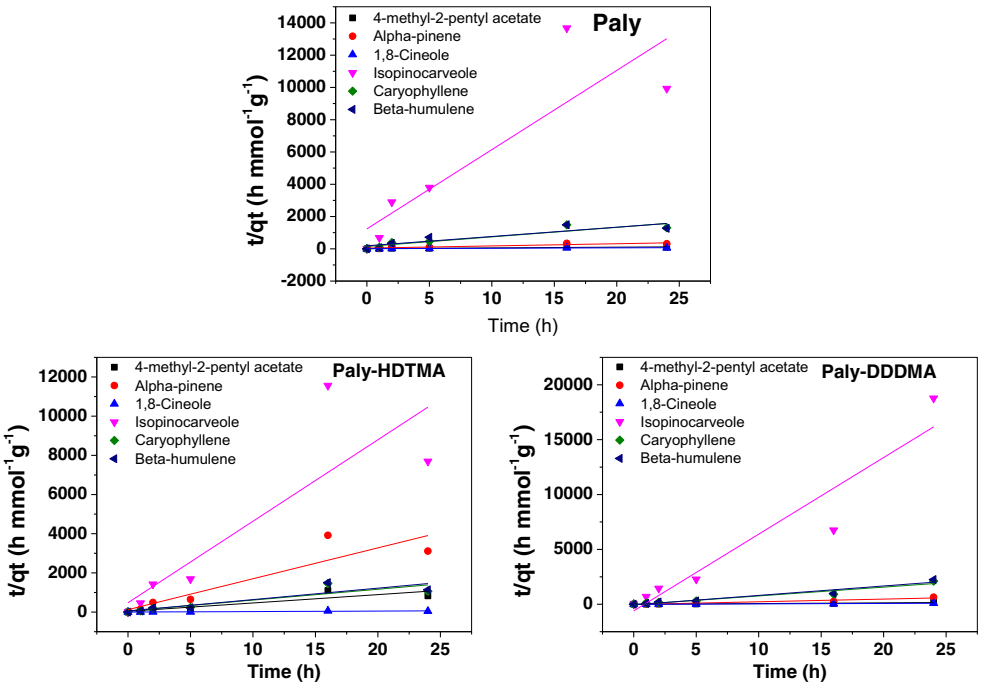

Fig. 10 Kinetic studies of pseudo-second-order of raw palygorskite and organo-palygorskites (Paly, Paly-HDTMA, and Paly-DDDMA)

Table 3 Adsorption rate constants obtained from pseudo-second-order model of TC

		R^2	q (mmol g^{-1})	$q_{exp.}$ (mmol g^{-1})	K_2
Paly	4-methyl-2-pentyl acetate	0.833	0.221	0.239	1802.538
	Alpha-pinene	0.797	0.074	0.077	4276.615
	1.8-cineole	0.842	0.377	0.411	1162.390
	Isopinocarveol	0.717	0.002	0.002	195,479.127
	Caryophyllene	0.826	0.017	0.018	24,198.252
	Beta-humulene	0.768	0.017	0.018	17,824.889
Paly-HDTMA	4-methyl-2-pentyl acetate	0.758	0.234	0.029	4602.118
	Alpha-pinene	0.792	0.063	0.007	19,557.164
	1.8-cineole	0.762	0.408	0.504	2668.929
	Isopinocarveol	0.679	0.002	0.003	363,152.637
	Caryophyllene	0.736	0.018	0.022	52,496.690
	Beta-humulene	0.758	0.017	0.021	62,215.424
Paly-DDDMA	4-methyl-2-pentyl acetate	0.911	0.149	0.228	9164.032
	Alpha-pinene	0.914	0.040	0.062	30,899.819
	1.8-cineole	0.921	0.266	0.395	5469.879
	Isopinocarveol	0.887	0.001	0.002	814,396.527
	Caryophyllene	0.935	0.012	0.017	142,990.919
	Beta-humulene	0.936	0.011	0.016	136,706.663

Secondly, the hydrophobicity of palygorskite increases after the attachment of DDDMA.

Moreover, the intraparticle diffusion model (Fig. 11) was less suitable for the experimental data if compared with the second-order kinetic model (Table 4). The curve does not pass through the origin. This indicates adsorption process is not limited by intraparticle diffusion of TC within Paly-DDDMA. Added these results obtained from intra-particular diffusion unlike for similar study (Nguemtchouin et al. 2015).

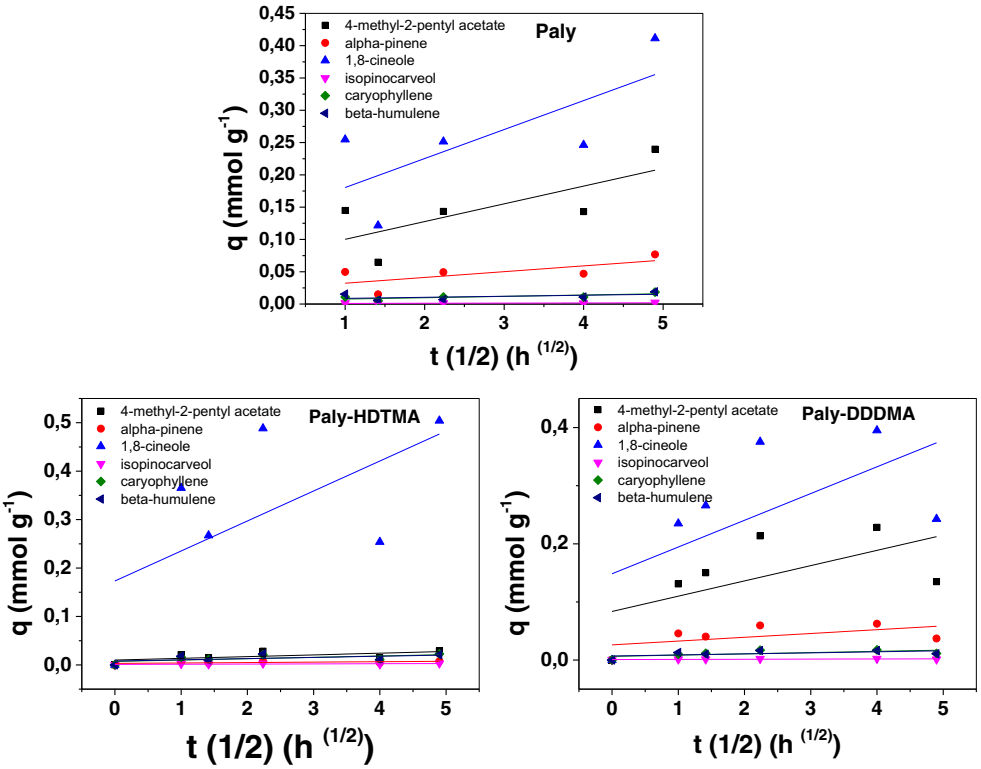

Fig. 11 Intraparticulaire diffusion kinetic model of TCOV adsorption onto raw palygorskite and organo-palygorskite (Paly, Paly-HDTMA, and Paly-DDDMA)

Table 4 Adsorption rate constants obtained from intraparticulaire order model of TC

		R^2	K_d	C
Paly	4-methyl-2-pentyl acetate	0.743	0.072	0.027
	Alpha-pinene	0.684	0.023	0.008
	1.8-cineole	0.732	0.135	0.044
	Isopinocarveol	0.652	0.0007	0.0002
	Caryophyllene	0.747	0.005	0.002
	Beta-humulene	0.486	0.007	0.001
Paly-HDTMA	4-methyl-2-pentyl acetate	0.615	0.01	0.003
	Alpha-pinene	0.543	0.003	0.0008
	1.8-cineole	0.619	0.173	0.061
	Isopinocarveol	0.610	0.0009	0.0003
	Caryophyllene	0.635	0.007	0.002
	Beta-humulene	0.538	0.008	0.002
Paly-DDDMA	4-methyl-2-pentyl acetate	0.603	0.083	0.026
	Alpha-pinene	0.542	0.026	0.006
	1.8-cineole	0.607	0.148	0.046
	Isopinocarveol	0.571	0.0008	0.0002
	Caryophyllene	0.637	0.006	0.002
	Beta-humulene	0.555	0.007	0.001

Conclusion

The current study investigated the use of organo-palygorskite for environmental applications in terms of attachments of TC from essential oil of Eg. Their structural properties of organo-palygorskite were examined using various techniques. In most studies of the surfactant intercalation on clay such as smectite, leading to expanded basal spacings (Hongping et al. 2004). But in our study, the intercalation of HDTMA and DDDMA were confirmed by FTIR analyses despite the interlayer space of the palygorskite were not increased (Yunfei et al. 2010). The organo-palygorskites were found to be more efficient for TC adsorption than the raw palygorskite due to the hydrophobicity properties acquired. The palygorskite interlaced with higher surfactant as well as those intercalated with DDDMA tend to afford better uptakes of the TC. Further, the adsorption mechanism fitted with pseudo-second-order model.

In perspective, isotherms and thermodynamic studies will be carried in order to confirm the kinetic study and, further, to improve the mechanism of the adsorption of the TC onto the fibrous Tunisian clay palygorskite.

References

Affouri A, Eloussaief M, Kallel N, Benzina M (2015) Application of Tunisian limestone material for chlorobenzene adsorption: characterization and experimental design. Arb J Geosci 8(12): 11183–11192

Allen SJ, Mckay G, Khader KYH (1989) Intraparticle diffusion of a basic dye during adsorption onto sphagnum peat. Env Pollut 56:39–50

Antonioa P, Iha K, Suárez-Iha MEV (2007) Kinetic modeling of adsorption of di-2-pyridylketone salicyloylhydrazone on silica gel. J Colloid Interface Sci 307:24–28

Balan E, Saitta AM, Mauri F, Galas G (2001) First principles modeling of the infrared spectrum of kaolinite. Am Mineral 86:1321–1330

Batish DR, Singh HP, Kohli RK, Kaur S (2008) Eucalyptus essential oil as a natural pesticide. For Ecol And Manage 256:2166–2174

Berenbaum MR (1995) The chemistry of defence: theory and practice. In: Thomas E, Meinwald J (eds) Chemical ecology: the chemistry of biotic interaction. National Academy of Science, Washington DC, p 224

Bradley WF (1940) The structural scheme of attapulgite. Am Mineral 25: 405–411

Brown ME (1988) Thermogravimetry in: introduction to thermal analysis: techniques and applications. Chapman and Hall, Springer London, pp 19–54

Brunauer S, Deming LS, Deming WE, Teller E (1940) On a theory of the van der Waals adsorption of gases. J Am Chem Soc 62:1723

Caillère S, Henin S, Rautureau M (1982) Minéralogie des argiles 2ème éd. Masson, Paris, pp 22–64

Dammak N, Ouledltaeuif O, Fakhfakh N, Benzina M (2014) Adsorption equilibrium studies for O-xylene vapour and modified clays system. Surf Interface Anal 46:457–464

Duke SO (1990) Natural pesticides from plants. Adv Nw Cor J Janick and J E Simon éd Timber press Portland Oregon USA 540

Eloussaief M, Kallel N, Yaacoubi A, Benzina M (2011) Mineralogical identification, spectroscopic characterization, and potential environmental use of natural clay materials on chromate removal from aqueous solutions. Chem Eng J 168:1024–1031

Galan E (1996) Properties and applications of palugorskite-sepiollite clays. Clay Min 31:443–453

Ghrab S, Boujelben N, Medhioub M, Jamoussi F (2014) Chromium and nickel removal from industrial wastewater using Tunisian clay. Desali Water Treat 52:2253–2260

Hamza W, Chtara C, Benzina M (2014) Characterization and application of Fe and iso-Ti-pillared bentonite on retention of organic matter contained in wet industrial phosphoric acid (54%): kinetic study. Res Chem Intermed 41:6117–6140

Han J, Liang X, Xu Y, Xu Y (2015) Removal of Cu^{2+} from aqueous solution by adsorption onto mercapto functionalized palygorskite. J Ind Eng Chem 23:307–315

Hassan SSM, Awwad SN, Aboterika AHA (2008) Removal of mercury (II) from wastewater using camel bone charcoal. J Hazard Mater 154:992–997

He H, Ma L, Zhu J, Frost RL, Theng BKG, Bergaya F (2014) Synthesis of organoclays: a critical review and some unresolved issues. App Clay Sci 100:22–28

Hongping H, Ray FL, Jianxi Z (2004) Infrared study of $HDTMA^+$ intercalated montmorillonite. Spectrochim Acta Part A 60: 2853–2859

Ibrahim S, Ang HM, Wang S (2009) Removal of emulsifed food and mineral oils from wastewater using surfactant modified barley straw. Bioresour Technol 100:5744–5749

Jarraya I, Fourmentin S, Benzina M, Bouaziz S (2010) VOC adsorption on raw and modified clay materials. Chem Geo 275:1–8

Juang RS, Lin SH, Tsao KH (2002) Mechanism of sorption of phenols from aqueouses solutions onto surfactants modified montmorillonite. J Colloid Interface Sci 254:234–241

Khalaf H, Bouras O, Perrichon V (1997) Synthesis and characterization of Al-pillared and cationic surfactant modified Al-pillared Algerian bentonite. Microporous Mater 8:141–150

Lee SY, Kim SJ (2002) Adsorption of naphthalene by HDTMA modified kaolinite and halloysite. App Clay Sci 22:55–63

Marras SI, Tsimpliaraki A, Zuburtikudis I, Panayiotou C (2007) Thermal and colloidal behavior of amine-treated clays: the role of amphiphilic organic cations concentration. J Colloid Interface Sci 315:520–527

Nguemtchouin MGM, Ngassoum MB, Kamga R, Lagerge S, Gastaldi E, Chalier P, Cretin M (2015) Characterization of inorganic and organic clay modified materials: an approach for adsorption of an insecticidal terpenic compound. Appl Clay Sci 104:110–118

Ozcan A, Sahin M, Ozcan AS (2005) Adsorption of nitrate ions onto sepiolite and surfactant-modified sepiolite. Adsorpt Sci Technol 23:323–334

Paré PW, Tumlinson JH (1996) Plant volatile signals in response to herbivore feeding. Fla Entomol 79:93–103

Park, Y., Godwin, A., Ayoko, Frost, R. L (2011). Characterisation of organoclays and adsorption of p-nitrophenol: environmental application. J Colloid Interface Sci 360, 440–456.

Qiu G, Xie Q, Liu H, Chen T, Xie J, Li H (2015) Removal of Cu (II) from aqueous solutions using dolomite–palygorskite clay: performance and mechanisms. App Clay Sci 118:107–115

Srihari V, Das A (2008) The kinetic and thermodynamic studies of phenol-sorption onto three agro-based carbons. Desalination 225:220–234

Torres-Pérez J, Solache-Rios M, Colin-Cruz A (2008) Sorption and desorption of dye Remazol Yellow onto Mexican surfactant-modified clinoptilolite-rich tuff and a carbonaceous material from pyrolysis of sewage sludge. Water Air Soil Pollut 187:303–313

Tuccimei P, Mollo S, Soligo M, Scarlato P, Castelluccio M (2015) Real-time setup to measure radon emission during rock deformation: implications for geochemical surveillance. Geosci Instrum Method Data Syst 4:111–119

Wang W, Wang A (2016) Recent progress in dispersion of palygorskite crystal bundles for nanocomposites. App Clay Sci 119:18–30

Wu FC, Tseng RL, Juang RS (2001) Kinetic modeling of liquid-phase adsorption of reactive dyes and metal ions on chitosan. Water Res 35:613–618

Xi Y, Mallavarapu M, Naidu R (2010) Adsorption of the herbicide 2, 4-D on organo-palygorskite. App Clay Sci 49:255–261

Yuan X, Li C, Guan G, Liu X, Xiao Y, Zhang D (2007) Synthesis and characterization of poly(ethylene terephthalate)/attapulgite nanocomposites. J App Polym Sci 103:1279–1286

Yunfei X, Mallavarapu M, Naidu R (2010) Adsorption of the herbicide 2, 4-D on organo-palygorskite. App Clay Sci 49:255–261

Zhou L, Chen H, Jiang X, Lu F, Zhou Y, Yin W, Ji X (2009) Modification of montmorillonite surfaces using a novel class of cationic gemini surfactants. J Colloid Interface Sci 332:16–21

Zhu R, Chen Q, Zhou Q, Xi Y, Zhu J, He H (2016) Adsorbents based on montmorillonite for contaminant removal from water: a review. App Clay Sci 123:239–258